This article has been accepted for inclusion in a future issue of this journal. Content is final as presented, with the exception of pagination.

Preflight Radiometric Calibration of the Orbiting Carbon Observatory

Christopher W. O'Dell, Jason O. Day, Randy Pollock, Carol J. Bruegge, Denis M. O'Brien, Rebecca Castano, Irina Tkatcheva, Charles E. Miller, and David Crisp

***Abstract*—This paper describes the radiometric calibration of the original Orbiting Carbon Observatory. The calibration process required characterizing both the dark current level and gain coefficients of each instrumental channel. The dark response was characterized with extensive testing and revealed some unexpected instrument behavior. The gain coefficients were characterized via illumination of the instrument spectrometers with a laboratory-calibrated integrating sphere source. Comparison between the spectrometer output and a calibrated photodiode led to a set of calibration coefficients for each spectrometer channel. The calibration coefficients were validated by a novel approach involving observation of the solar spectrum through a transmission filter. Validation occurred by examination of both the ratio of the filtered to unfiltered spectra and retrievals of geophysical quantities such as surface pressure. The linearity of the calibration was established to approximately 0.2%. Finally, using the calibration data from the integrating sphere, a simple noise model was developed for each channel of the instrument. A summary of the signal-to-noise performance is included.**

***Index Terms*—IEEEtran, journal, LaTeX.**

I. Introduction

The ORBITING Carbon Observatory (OCO) was a National Aeronautics and Space Administration (NASA) Earth System Science Pathfinder mission designed to measure global CO_2 concentrations twice a month with the precision and accuracy required to detect sources and sinks on regional scales [1], [2]. It was launched on February 24, 2009, but did not achieve orbit due to a failure of the launch vehicle. However, the details of its preflight calibration are relevant both in their own right, as well as in relation to the successor mission OCO-2, planned for launch in 2013.

This paper addresses the preflight radiometric calibration of the original OCO instrument, performed during thermal-vacuum testing in 2007 and 2008 at the Jet Propulsion Laboratory (JPL), Pasadena, CA. The spectral calibration of the instrument is described in a companion paper [3]. Initial details of the calibration were previously given in [4]. This work provides more details on the derivation of the dark response model and gain coefficients to be used in flight and also provides a simple validation approach that was used to test and refine the calibration.

This paper is organized as follows. Section II provides a description of the instrument. Section III describes the initial preflight calibration methodology, including the characterization of the instrument dark response, gain coefficients, and an assessment of the calibration using ground-based solar observations. This initial calibration proved insufficiently accurate to meet the OCO mission requirements; a refinement of the calibration gain coefficients and their assessment are described in Section IV. Results of the resulting laboratory-measured signal-to-noise ratio (SNR) are given in Section V, followed by concluding remarks in Section VI.

II. Instrument Overview

The OCO instrument was used to measure the sunlight reflected by the surface and atmosphere of the earth in three narrow bands. The oxygen A-band measured absorption by molecular oxygen near 0.76 μm, while two carbon dioxide bands, termed as weak and strong CO_2 bands, were located near 1.6 and 2.0 μm, respectively. A sample spectrum of the sun taken with the flight instrument on February 26, 2008, is shown in Fig. 1. The spectral range of each channel included the complete molecular absorption band, as well as some nearby continuum to provide constraints on the optical properties of the surface and aerosols, as well as absorbing gases [1].

The instrument consisted of three imaging spectrometers, one for each band [5], as shown in Fig. 3. Light was directed into the spectrometers through a common telescope and a series of beam splitters and reimagers. Just before the incoming light enters each spectrometer, a linear polarizer selects the polarization vector parallel to the entrance slit. Each spectrometer worked in the first order and used a flat holographic grating.

At each spectrometer's focus, an area array collects the spectrum. As is typical in imaging spectrometers, one dimension measured field angles along the slit, and the other dimension measured different wavelengths. The detectors were 1024 × 1024 arrays; the O_2 A-band was silicon (HyViSI) Hawaii-1RG, and the two CO_2 detectors were HgCdTe Hawaii-1RG; all were manufactured by Teledyne Scientific and Imaging, LLC. Only 160 pixels in the spatial dimension were used out of the 1024. Sets of 20 were averaged onboard to yield eight spatial

Manuscript received May 6, 2010; revised July 15, 2010; accepted August 22, 2010.

C. W. O'Dell and D. M. O'Brien are with the Cooperative Institute for Research in the Atmosphere, Colorado State University, Fort Collins, CO 80523-1375 USA (e-mail: odell@atmos.colostate.edu; obrien@atmos.colostate.edu).

J. O. Day was with the Department of Atmospheric Science, Colorado State University, Fort Collins, CO 80523-1371 USA. He is now with the National Science Foundation, Washington, DC 20006-4403 USA.

R. Pollock, C. J. Bruegge, R. Castano, I. Tkatcheva, C. E. Miller, and D. Crisp are with the Jet Propulsion Laboratory, California Institute of Technology, Pasadena, CA 91109-8099 USA.

Color versions of one or more of the figures in this paper are available online at http://ieeexplore.ieee.org.

Digital Object Identifier 10.1109/TGRS.2010.2090887

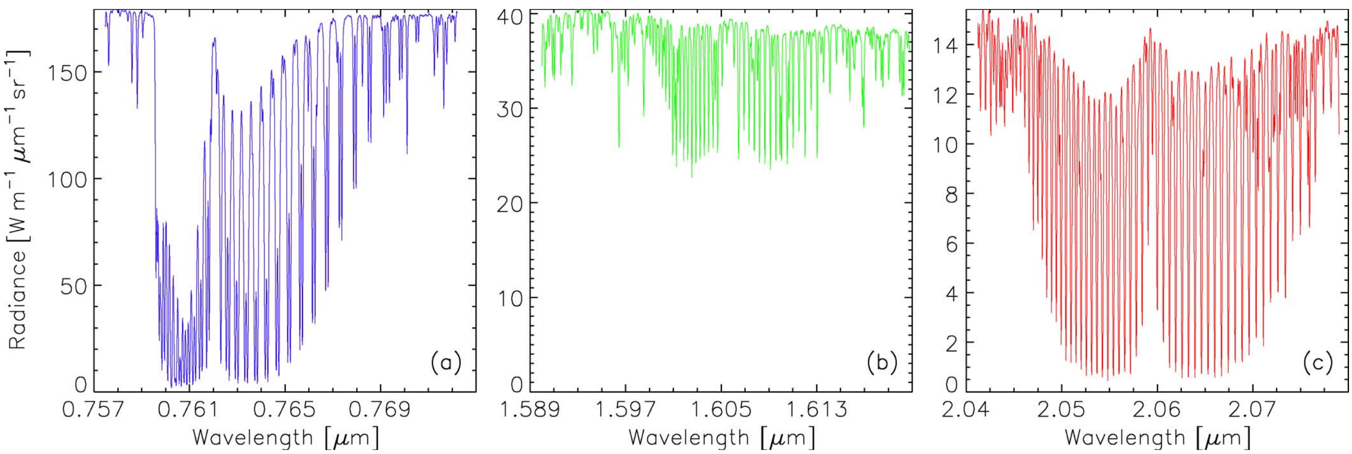

Fig. 1. Sample spectra from the OCO instrument taken from the ground on February 26, 2008; the solar zenith angle was approximately 39°. The band near (a) 0.76 μm measured O_2 absorption, while the bands depicted in (b) and (c) measured absorption by carbon dioxide and are referred to as the weak and strong CO_2 bands, respectively.

footprints; each would have had a 1.5-km field of view on the ground. In the spectral dimension, four pixels were blacked out on each side of the array, leaving 1016 pixels (or channels) per band. The OCO detectors were cooled to 180 K (O_2 A) and 120 K (weak CO_2, strong CO_2) and actively controlled to within ± 1 K. This minimized gain and dark current changes due to temperature drifts.

To measure accurately the depth of each absorption line and accurately retrieve gas and aerosol information, both absolute and relative radiometric calibrations are essential. The calibration goal for OCO was better than 5% absolute accuracy, better than 1% relative accuracy between the three bands, and better than 0.1% relative accuracy among channels within a band. To check the calibration standards used by OCO, a cross-calibration experiment was conducted with the Japanese team building the Greenhouse gases Observing SATellite (GOSAT) [4]. This experiment showed agreement of the independent calibration standards to better than 3.0% in all three OCO bands. The relative calibration consistency between the three bands and among channels within a single band was not tested by this experiment.

For carbon dioxide retrievals, the requirement of 0.1% intraband relative accuracy is probably both the most important and the most difficult to achieve. Undiagnosed nonlinearities in the spectrometer response can easily lead to calibration errors larger than this. Characterizing detector nonlinearity requires calibration over a wide range of input intensities. In a traditional radiometric calibration, the number of tested intensity levels, the stability of the calibration system, and the length of observations at each intensity level can create a test of impractical durations. Practical considerations limited the OCO radiometric calibration tests to $\sim$24 h each.

III. Calibration Methodology

The OCO instrument was calibrated prior to its installation into the spacecraft bus; testing was conducted from August 2007 through February 2008. At that time, the radiometric, spectral, and geometric properties were established. All tests were performed in a 3-m thermal-vacuum chamber at NASA's JPL, simulating the on-orbit environment. Radiometric testing provided a measure of the instrument's SNR; the zero level (dark current) offset; the absolute, detector-relative, and spectrometer-relative gains; and gain linearity. It also identified bad pixels, creating a table of data elements to be omitted in science processing.

The OCO instrument detected light in only one polarization component; it was sensitive to a particular linear combination of Stokes parameters I, Q, U, and V. Specifically, because OCO only detected the polarization component parallel to the slit direction, it measured

$$I_{\mathrm{meas}} = I - Q_{\mathrm{slit}} \tag{1}$$

where Q_{slit} is defined with respect to an $x{-}y$ coordinate system, where $\hat{y}$ is parallel to the entrance slit. It was assumed that each OCO channel for each of the eight footprints could be described by a response of the form

$$DN_{ij}(I) = DN_{0,ij} + c_{1,ij} I_{\mathrm{meas}} + c_{2,ij} I_{\mathrm{meas}}^2 \tag{2}$$

where $c_{1,ij}$ and $c_{2,ij}$ are the gain coefficients for spectral channel i and footprint j, respectively, $DN_{ij}(I)$ is the observed "digital number" of counts for input intensity I, and $DN_{0,ij}$ is the dark current level. Once the dark current level and gain coefficients were known, the I_{meas} value for any observation and in any channel could be derived from the observed DN simply by inverting (2). During calibration, the coefficients c were determined with an unpolarized light source. However, on-orbit data would have only provided the calibrated I_{meas} quantity rather than the unpolarized intensity I. It would have been the data user's responsibility to take into account OCO's polarization sensitivity in their work. This requires knowing the slit orientation for each sounding, leading to a more useful version of (1), i.e.,

$$I_{\mathrm{meas}} = I + Q \cos 2\phi_p + U \sin 2\phi_p \tag{3}$$

where ϕ_p denotes an instrument quantity called the polarization angle and is related to the slit orientation relative to the principal plane; this quantity would have been provided with the OCO

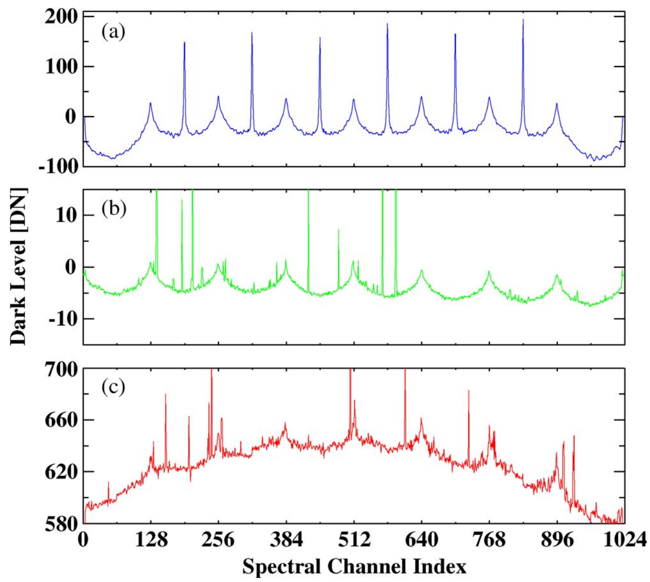

Fig. 2. Typical dark current response in each band from the OCO instrument. (a) O_2 A-band. (b) Weak CO_2 band. (c) Strong CO_2 band.

calibrated radiance. For observations in the principle plane, $\phi_p = \pi/2$.

A. Dark Current Assessment

The first step in calibration was to determine the instrument response in the absence of an input radiation source; this was referred to as the dark current response or simply as the "dark." It is represented as $DN_{0,ij}$ in (2). To understand the dark response, it is first necessary to go into a bit more detail on the OCO instrument and data readout method. Each instrument measurement is due to two different reads: a "pedestal" value and an integrated value. The actual returned signal in DN is integrated minus pedestal; this was referred to as a correlated double-sample (CDS) pair. A very large background pattern was found to be present in both the pedestal and integrated values; upon subtraction, this pattern (termed as W-pattern due to the shape) does not entirely cancel out even in the dark. The residual DN_0 still has features of the W-pattern. Fig. 2 shows a typical dark response (integrated minus pedestal) taken during thermal-vacuum testing for each OCO band, which, in this case, is for instrument footprint four.

The repetitive structure seen every 64 pixels in the figure is due to the detector readout scheme. Sixteen multiplexers were used to read out each detector row; each multiplexer thus read 64 of the 1024 pixels. It is believed that the heating in each multiplexer during a read cycle is largely responsible for the cyclic pattern seen in the dark response of each band. Notice also that the CDS pairs are sometimes less than zero. The spikes seen in the two CO_2 bands are due to bad pixels in the detector arrays. These bad pixels would have been masked out for actual flight data.

Classical photodiodes have a dark response that is dominated by a thermal term that is a function of detector temperature; for these detectors, the thermal term is expected to be on the order of one count. The patterns due to the peculiarities of the OCO readout scheme shown in Fig. 2 have amplitudes of several counts in the weak CO_2 band to several hundred counts in the O_2 A-band. Because the dark level would only be measured once per orbit in flight, it was necessary to discover if any dependences on instrumental characteristics (such as temperature) were present in these dark response patterns, such that the dark changes induced by instrumental changes occurring within a single orbit could be removed.

The O_2 A-band detector dark response was found to have dependence only on the detector temperature. For almost all the pixels, the sensitivity to detector temperature was very weak, which is around 0.4 DN/K. Considering that the temperature would be controlled on orbit to ± 1 K, this dependence would be of no importance. However, pixels near or on the multiplexer boundaries had much higher sensitivities, from 30 to 80 DN/K. Fortunately, this dependence was found to be well described by a simple linear function. On orbit, the detector temperatures would have been measured continuously; dark current changes associated with the changes in detector temperature could be calculated and subtracted out on a frame-by-frame basis. Drifts in the A-band dark current not associated with the detector temperature were significantly less than one count per hour.

In contrast to the A-band, the weak CO_2 band dark response was not found to depend significantly on any environmental variable. Thus, a constant model of the dark response was adopted for that band. In flight, the weak CO_2 band dark response would be measured in every orbit to monitor its stability.

The dark response in the strong CO_2 band was found to contain a significant emission term of 580–640 counts. We performed a calculation of the blackbody radiation from the optical bench at its nominal temperature of -6 °C, taken together with a rough internal model of the instrument that determines how many such photons would fall on each detector element. This simple calculation yielded a theoretical expectation of 548 counts of dark response per detector, within $\sim$20% of the value observed. However, each detector element was a little bit different; thus, the actual sensitivities to optical bench temperature were also measured explicitly. We found sensitivities of 50–70 DN/K, roughly consistent with the calculated thermal emission from the optical bench (54 DN/K).

Three simple models of dark response were therefore adopted: linear in detector temperature for the O_2 A-band, constant for the weak CO_2 band, and linear in optical bench temperature for the strong CO_2 band. These models were validated using a set of 42 dark observations taken at essentially random times throughout the two-week period of thermal-vacuum testing. These dark observations contained a much larger variation in instrumental temperatures, voltages, and other conditions than would be observed in flight. The root-mean-square errors of the model-predicted dark value in each of the three bands were found to be approximately 4, 3, and 6 DN, respectively. On-orbit errors in the dark level would have been much smaller than this because the instrumental dark typically drifted by a few tenths of a fount or less per hour. Because the instrument dark would be bounded by darks measured once per orbit, with suborbit dark changes modeled as described earlier, dark errors could be expected to be at most a few tenths of a count. This leads to negligible calibration errors in the

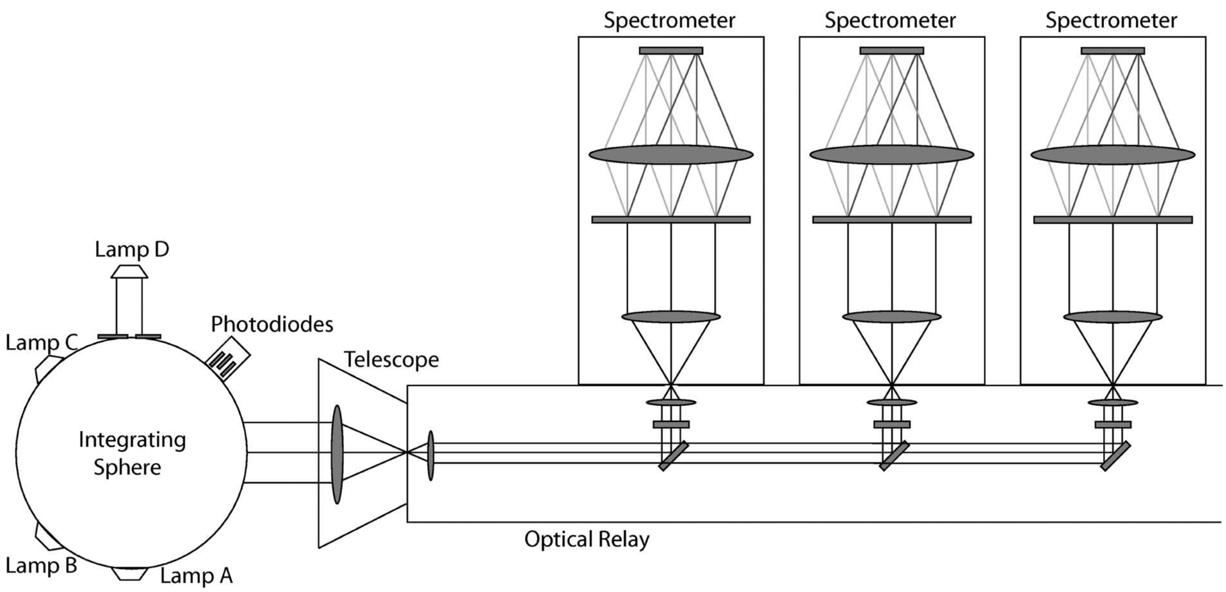

Fig. 3. Schematic showing the OCO spectrometer optics chain, as well as the integrating sphere for the radiometric test. Lamp D is external to the integrating sphere, and its brightness is controlled by an adjustable slit. The drawing is not to scale.

continuum and errors of at most a few tenths of a percent deep in line cores for scenes of typical brightness.

B. Measurement of Gain Coefficients

The details of the calibration test equipment and the approach for the measurement of gain coefficients are summarized hereinafter; see [4] for a more complete description. For preflight radiometric testing, OCO used an 89-cm-diameter integrating sphere with a 20-cm-diameter exit port. The interior of the sphere was coated with Eastman Kodak material 6080, which is essentially barium sulfate. A schematic of the test setup is shown in Fig. 3. The sphere was external to the thermal-vacuum chamber and fully illuminated the instrument entrance slit through a window. Four tungsten bulbs illuminated the sphere: three internal (lamp A: 35 W, lamp B: 75 W, and lamp C: 75 W) and one external (lamp D: 1000 W). There was a variable slit between the external lamp-D source and the entrance aperture to the sphere. Using the bulbs in various combinations, along with the external source slit, a range of output illuminations was achieved. In all, there were 30 illumination levels used in the OCO test plan, spanning the dynamic range of each OCO band.

The sphere was purged while in operation with dry nitrogen to eliminate absorption by CO_2, O_2, and H_2O that would otherwise introduce spectral features in the incident light. Three monitoring photodiodes were used with the sphere, one for each of the OCO channels. An external carousel rotated each of the three photodiodes into place, one at a time. The intensity incident on the OCO instrument was determined from the photodiode output. The output was reported in absolute radiance units, traceable to a standard of the National Institute of Standards and Technology. The monitoring photodiodes were used to transfer the radiometric scale from the lamp standard to the OCO instrument. For this reason, the photodiodes were also known as "transfer radiometers."

The photodiodes were developed and fabricated at JPL for use on OCO. A custom baffle tube is the first component and limits the field of view to 5°. Next, a passband filter modifies the light that passed through the detector. A commercial detector is the last light-sensitive component. The photodiodes were initially tested for gain, linearity, and spectral and radiometric responses; however, some refinements to the photodiode proved to be necessary, as discussed in Section IV.

The calibration tests were conducted by turning on or off each of lamps A, B, and C and then varying the slit width to lamp D (see Fig. 3) to produce a range of intensity values spanning the dynamic range of the spectrometers. Each lamp state was maintained for 3 min so that the signal from each of the channels (which have a 0.334-s frame rate) could be averaged. This ensured that the radiance from the sphere had reached equilibrium.

The calibration took place in two steps. First, the light level used was converted to radiance by assuming the photodiode response to be linear, i.e.,

$$V(S) = V_0 + d_1 I_{PD}(\lambda_0) \tag{4}$$

where V was the voltage measured at a given intensity $I_{PD}(\lambda_0)$ incident upon the photodiode, and d_1 and V_0 were the predetermined parameters of the photodiode in question. λ_0 is the independently measured centroid wavelength of response of each photodiode.

It was then assumed that the intensity incident upon the OCO flight instrument at the centroid wavelength $I(\lambda_0)$ was equal to the intensity incident upon the photodiode $I_{PD}(\lambda_0)$. This assumption is examined in Section IV. Finally, the intensity incident upon the OCO instrument at an arbitrary wavelength λ in a given band was computed according to

$$I(\lambda) = I(\lambda_0)\phi(\lambda) \tag{5}$$

where $\phi(\lambda)$ represents the relative spectral dependence of the intensity field inside the sphere for a given band. It was defined via simultaneous measurements of the intensity field by an Analytical Spectral Devices (ASD) FieldSpec Pro spectrometer, as described in detail in [4].

C. Evaluation of the Initial Calibration

The absolute calibration of the OCO instrument was partially verified by in-laboratory comparison to the GOSAT instrument [4]. For each band, the absolute calibration of each instrument was found to agree to better than 3%. However, OCO mission requirements stated that channels within an individual band must have relative calibration errors of less than 0.1%. The OCO test plan provided a unique method of testing the validity of (2) fits that proved crucial to the final validation of the radiometric calibration and specifically to validating the intraband relative calibration.

In order to evaluate the intraband calibration, and particularly the errors in the description of the calibration nonlinearity for each channel, the following procedure termed as "matador test" was used. A series of mirrors directed light from the sun, appropriately filtered so that the instrument would not saturate, onto the entrance slit of the spectrometers. In addition, a special sheet was optionally inserted into the optical path to let through a fraction of the solar intensity. To create a spectrally uniform reduction in the solar intensity reaching the instrument, an aluminum sheet with ~3-mm holes was inserted into the heliostat optical path. The holes were arranged in a hexagonally packed pattern with an approximately 50-fill factor (to let through approximately 50% of the light). These holes were large enough to ignore diffraction, but small enough to ensure that the entrance telescope was well sampled. This sheet was rapidly inserted or removed every 30 s and tested the instrument's response to rapid changes in the light level [6], as well as providing a spectrally flat change of the light level entering the instrument.

This "matador test" (so named because the motion of the sheet suggests a visual analogy to a matador's cape) was used to test the radiometric calibration coefficients of the spectrometer channels by taking the ratio of the unfiltered radiance levels to the filtered levels. The absorption lines ensured that the ratios covered radiance that spanned the dynamic range of the instrument. If the spectrometer channels were properly calibrated, the intensity ratio would be constant regardless of the channel or equivalent to the radiance level.[1] As an aside, the original purpose of this test was actually to measure any residual image in the focal plane arrays. Early testing showed that the O_2 A-band detector only displayed residual image in the presence of sharp spectral features [6].

The results of the matador test can be seen in Fig. 4, with the ratio plotted against the relative intensity of each channel. Again, one would expect that a perfectly calibrated instrument would have a constant ratio over all relative intensity values and across all three bands. As the data in Fig. 4 show, this is not the case. The strong CO_2 band is the worst, where the intensity ratio is around 0.48 at low radiance and increases to 0.50 at high radiance, well outside of the tolerance for the experiment. The scatter is also unacceptably large and is due primarily to the ratio's dependence on wavelength (or channel position). The weak CO_2 band and the O_2 A-band are both slightly bowed at lower radiance levels and also have ratios that differ by about 0.02, a difference which also exceeds the tolerance for the instrument calibration.

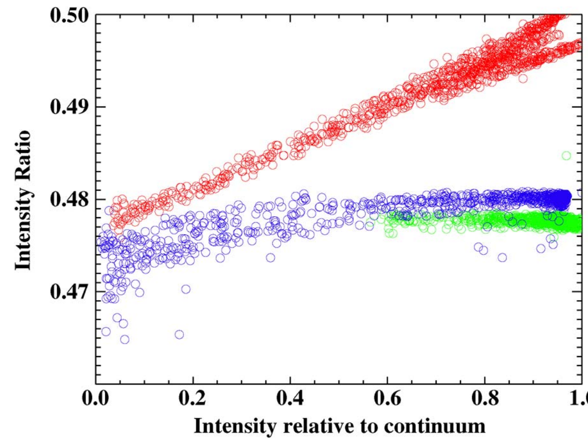

Fig. 4. Results of the initial ratio test. A 50% transmission sheet was inserted into the path of the sunlight that fell on the instrument. The figure shows the ratio of the full-intensity spectrum to the attenuated spectrum as a function of the relative intensity. The O_2 A-band is shown in blue, the weak CO_2 band in green, and the strong CO_2 band in red. The strong CO_2 band performance is the worst, with the ratio changing by 2% over the dynamic range of the spectrometer.

IV. Correction of Calibration Errors

The failure of the ratio test was due primarily to two faulty assumptions in the initial calibration procedure. The first assumption was that the response of the photodiodes to input intensity (4) was both linear and well characterized. Second, as stated previously, it was assumed that the intensity within the integrating sphere over the spectral range of OCO was uniform for all directions and locations within the sphere. Equivalently, it was assumed that the intensity incident upon the photodiodes I_{PD} was equal to the intensity I incident upon the OCO instrument. As explained hereinafter, the first assumption was found to fail for both the O_2 A-band as well as the strong CO_2 band. The second assumption was found to fail primarily for the strong CO_2 band.

A. O_2 A-Band Photodiode Calibration

In the O_2 A-band, the radiance that reached the photodiode was large enough that saturation effects were seen in the photodiode signal. This was verified by calculating the proportional signal increase on the photodiode between two lamp-D slit widths with all other lamps constant. For example, the difference in the photodiode current between a closed lamp-D slit and a 25% open slit should be the same with lamp A on, as it is with lamps A and B on. When lamps A, B, and C were all on, however, the current increase between these slit widths was smaller than it was at all other lamp states. This saturation effect

[1]The ratio was only known to be approximately 50% *a priori*, but could be slightly more or less due to the uncertainties in the machining process.

This article has been accepted for inclusion in a future issue of this journal. Content is final as presented, with the exception of pagination.

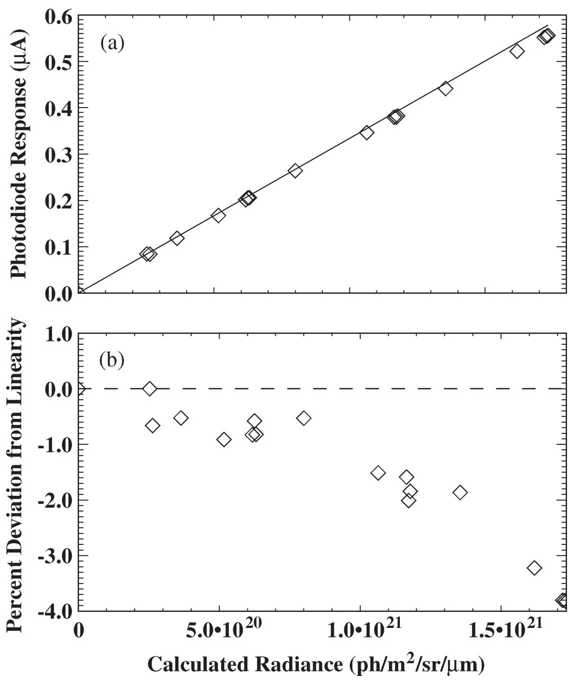

Fig. 5. Nonlinearity in the O_2 A-band photodiode response. (a) Photodiode partially saturates at high radiance levels. The black diamonds are photodiode observations, while the black line is the linear extrapolation of the signal. (b) Percent difference from linearity of the response.

was accounted for by replacing the linear photodiode response from (4) with a quadratic response

$$V = V_0 + d_1 S + d_2 S^2 \tag{6}$$

where V_0 is the background (dark) photodiode response, and d_1 and d_2 are the linear and quadratic components of the photodiode response. S represents an approximation to the total intensity incident upon the photodiode of the form

$$S = f_A S_A + f_B S_B + f_C S_C + f_D S_D \tag{7}$$

where f_X is the fraction of the full-intensity value of any lamp X that reaches the photodiode. For lamps A, B, and C, this value could only be zero or unity, while for lamp D, it could vary continuously from zero to one. Because the calibration procedure contained roughly 30 intensity levels (through different values of f_X), it was possible to solve simultaneously for the individual lamp intensities S_A, S_B, S_C, and S_D, as well as the photodiode parameters d_1 and d_2.

Fig. 5(a) shows the O_2 A-band photodiode response as a function of the calculated intensity derived from (7). The photodiode response is seen to differ from a linear extrapolation of the low-intensity response (red line) by up to 4% at the highest intensity levels [Fig. 5(b)].

B. Strong CO_2 Band Photodiode Calibration

The procedure of the previous section was repeated for the other two photodiodes as well. The weak CO_2 response was found to be linear and well characterized, but the strong CO_2 response was not linear and was not well fit by a simple quadratic response. The issues were found to be not related to saturation

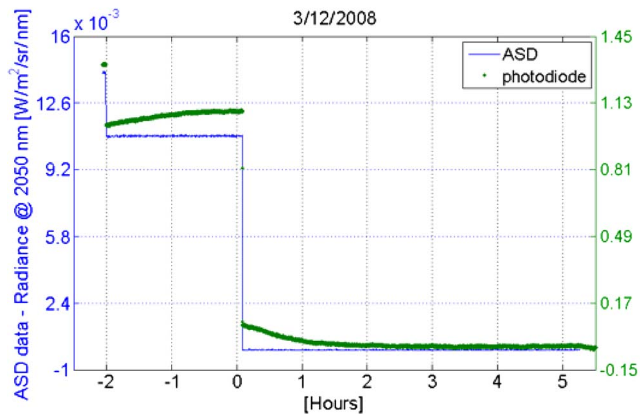

Fig. 6. Response of the strong CO_2 band photodiode is seen to lag behind the simultaneous reading of an ASD spectrometer when the lamps are switched on and then off. This was an indication that a variable dark current offset was induced by the heating of the sphere by the lamps.

but rather to a dark current offset [V_0 in (4)] that varied with the photodiode housing temperature. This was observed by turning all of the lamps on for 2 h and then off. The signal, shown in Fig. 6, comes down to a level above the dark current and then slowly recedes to the dark level over an hour. It is likely that the temperature controller on the photodiode did not adequately stabilize the thermal load from the integrating sphere, particularly at the highest intensity levels. As the light level changed, so too did the thermal load and, thus, the dark current offset.

Unfortunately, neither the photodiode housing temperature nor the integrating sphere temperature was recorded during the calibration procedure. Therefore, a model for the temperature effect was derived as follows. The temperature was assumed to be a simple function of the current light level plus several previous light levels. This was required because the rethermalization time for the sphere was around 30 min, whereas the lamp state was changed every 6 min. The offset associated with heating from past lamp states was assumed to dissipate with an exponential profile. The model for the photodiode response at time t_0 was assumed to follow

$$V = d_0\left(1 + \alpha \Delta T(t_0)\right) + d_1 S(t_0) \tag{8}$$

where d_0 represents the initial offset (found to be nearly zero), α is the scaling factor for the dark current offset, d_1 is the linear term (which should be nearly unity), and S is the intensity at t_0. ΔT is a purely empirical quantity assumed proportional to the photodiode housing temperature offset, i.e., the amount by which it was above its target value, assumed to be the temperature when the sphere was dark. ΔT at t_0 was modeled as a moving average of the previous lamp states (t_{-1}, t_{-2}, t_{-3}, etc.) at time zero of the form

$$\Delta T(t_0) = S(t_{-1})e^{-\Delta t/\tau} + S(t_{-2})e^{-2\Delta t/\tau} + \cdots + S(t_{-n})e^{-n\Delta t/\tau}. \tag{9}$$

Here, τ is a parameter describing the thermal time constant of the system, Δt is the average time between intensity states, and n is the number of previous states included in the average. $n = 5$ was found to yield a suitable fit.

This article has been accepted for inclusion in a future issue of this journal. Content is final as presented, with the exception of pagination.

TABLE I
DERIVED GEOMETRY FACTORS FOR EACH LAMP AND BAND

Band	G_A	G_B	G_C	G_D
O_2 A	0.9985	0.9892	0.9965	1.0
weak CO_2	0.9927	0.9897	0.9983	1.0
strong CO_2	0.9837	1.0131	1.0322	1.0

C. Integrating Sphere Uniformity

We now address the question of uniformity of the integrating sphere. The internal $BaSO_4$ coating was likely highly Lambertian and had a high reflectivity in the O_2 A-band of roughly 98% based on the measurements of Avian-B from Avian Technologies. These same measurements indicate lower reflectivities of approximately 92% and 81% in the weak and strong CO_2 bands, respectively. The result was that the light exiting the sphere did not bounce as many times at longer wavelengths, and spatial uniformity was compromised. This could lead to a slight intensity difference between the photodiode port and the exit port of the sphere. This intensity difference would, in principle, differ for each internal lamp due to the relative positioning within the sphere.

This effect was modeled by attributing to each lamp a multiplicative "geometry factor" that described the relative intensity difference at the two locations. This was incorporated into the model by modifying (7) as follows:

$$S = f_A S_A G_A + f_B S_B G_B + f_C S_C G_C + f_D S_D G_D \qquad (10)$$

where G_A, G_B, G_C, and G_D are the geometry factors that describe the difference between the intensity from each lamp observed at the photodiode and that observed at the spectrometer. The factor for lamp D was set to unity to prevent the geometry factors from scaling the instrument gain. It was assumed that each geometry factor was constant across a band. After correcting the photodiode response as described earlier, each spectrometer channel was fit separately for the four geometry factors and simultaneously for the OCO calibration coefficients $c_{1,i}$ and $c_{2,i}$ for each channel. The resultant geometry factors are shown in Table I. The inclusion of geometry factors in these fits made the fit residuals of the integrating sphere measurements 20%–50% better than fitting without geometry factors.

D. Evaluation of the Revised Calibration

It should be first emphasized that the changes made to the calibration methodology were based upon observed errors in the calibration test data rather than an attempt to yield consistently flat ratios in the matador test; thus, the ratio test acts as an independent validation of the calibration. It was found that the inclusion of lamp geometry factors made little difference in the O_2 A-band and actually made the weak CO_2 band slightly worse. Therefore, for the final calibration, geometry factors were not used (i.e., were set to unity) in these bands. This meant that the calibration for the weak CO_2 band was unchanged from the original.

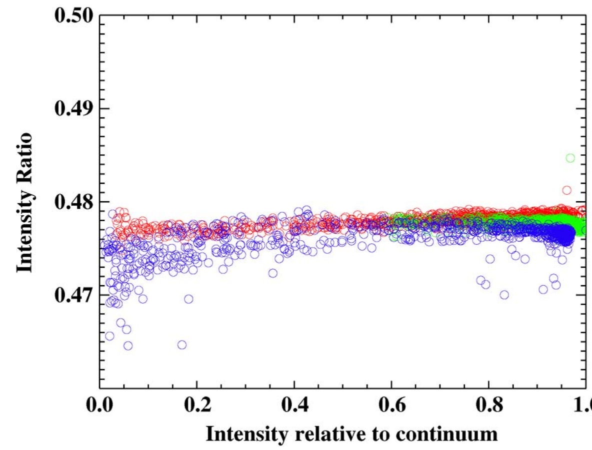

Fig. 7. Results of the ratio test performed with the revised calibration coefficients. The ratio is seen to be more consistent over the dynamic range of the three spectrometer bands. Color scheme is the same as for Fig. 4.

TABLE II
STATISTICS OF THE INTENSITY RATIO†

	Ratio Mean	Ratio Std. Dev.	Ratio Slope‡
Band 1 Original	47.9%	0.24%	0.55%
Revised	47.6%	0.16%	0.19%
Band 2 Original	47.7%	0.08%	-0.10%
Band 3 Original	49.2%	0.57%	2.23%
Revised	47.8%	0.06%	0.18%

† Ratio of filtered to unfiltered sunlight intensity in the matador test.
‡ Change in intensity ratio from relative intensity 0 to 1.

The results of the ratio test with the revised calibration coefficients can be seen in Fig. 7. As compared with the original coefficients in Fig. 4, the ratio of the filtered to unfiltered signal is clearly flatter with the new coefficients. The three bands show good agreement on the transmission of the "matador" cape at approximately 47.7%. The large slope on the strong CO_2 band ratio is now mostly gone, and the "trifurcation" originally observed in this band has also disappeared. Finally, despite some scatter at the low-intensity points, the O_2 A-band does not bow in Fig. 7 as much as it did in Fig. 4, although some bowing is, unfortunately, still present. The scatter seen in the figure is possibly due to instrument noise or imperfect characterization of the dark current.

Some statistics of the ratio test are shown in Table II. The standard deviation of the (low/high) intensity ratio is 0.16% in the O_2 A-band and less than 0.1% in the two CO_2 bands. Perhaps more importantly, the curves in Fig. 7 are now relatively flat, and their slopes show changes of less than 0.2%. The outlier points in the O_2 A-band for higher relative intensity values are channels on or near multiplexer boundaries; these channels proved difficult to characterize accurately.

To test the success of the revised calibration further, both old and new gain coefficients were used to perform simple gas retrievals on the same matador test data used in the ratio test. Specifically, 990 soundings were taken at a 3-Hz sampling rate, with the 50% filter inserted and removed roughly every 30 s.

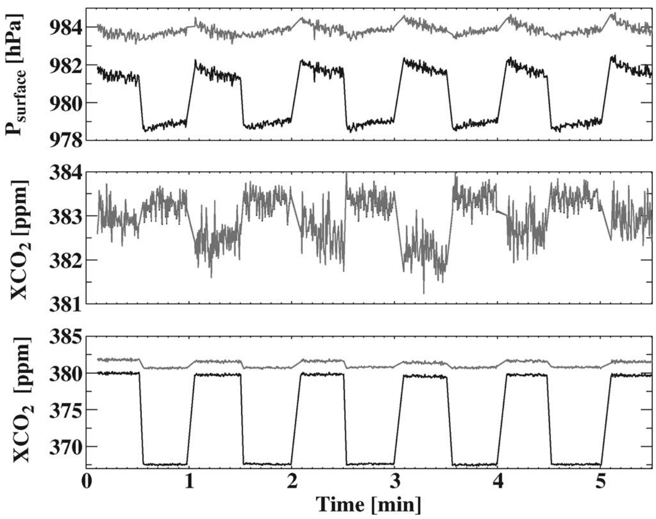

Fig. 8. Single-band retrievals performed with (black) the original radiometric calibration and (gray) the revised calibration on several minutes of matador test data. The light level was varied between ∼50% and 100% sunlight, with approximately 30 s spent in each state. Three seconds of data have been removed around each transition to remove the data of poor quality. The top panel shows the O_2 A-band retrieval of surface pressure (in hectopascals), while the middle and bottom panels show the retrieval of X_{CO_2} (in parts per million) using the weak and strong CO_2 bands, respectively. Note that 10 ppm has been added to the strong CO_2 band, original calibration retrieval for clarity. The weak CO_2 band calibration was not changed from the original.

Because the ratio of the unfiltered to filtered spectra has identical spectral features, retrievals of X_{CO_2} and surface pressure P_{surf} should be identical for both the unfiltered and filtered spectra. A separate retrieval was performed for each band and sounding, specifically on instrument footprint 4. The retrieval was based on optimal estimation, as described, for example, in [7]. The basics of the forward model have been described previously in [8]. The spectroscopy is based on HITRAN-2008 [9], with line mixing in the O_2 A-band and strong CO_2 band included according to [10] and [11]. The spectral response functions and positions are described in a companion paper [3].

In the O_2 A-band, there were four retrieved parameters: surface pressure, an offset to a predefined temperature profile, and the mean and the slope of the continuum level. In the two CO_2 bands, there were five retrieved parameters: X_{CO_2}, temperature offset, the two continuum parameters, and a scale factor to a predefined water vapor profile. To the best of our knowledge, differences in the retrievals between half- and full-sunlight observations are indicative only of calibration errors, as nothing else changed appreciably over the course of the experiment. Errors in the forward model, such as in spectroscopy or instrument line shape function, should lead only to biases, not to retrieval differences between the full- and half-sunlight exposures.

The results of the retrievals can be seen in Fig. 8. The original calibration results are shown in black, while the revised calibration results are in gray. In the O_2 A-band (upper panel), the surface pressure retrievals exhibit a roughly 3-hPa difference between the two sunlight states, which decreases to ∼0.3 hPa for the revised calibration. Because this error is due to slightly incorrect characterization of the instrument nonlinearity, it is likely that the error would only marginally increase for even dimmer scenes.

In the weak CO_2 band (middle panel), the retrieved X_{CO_2} differs by about 0.7 ppm, or 0.2%, between the two intensity states. As stated previously, the calibration with geometry factors actually made these results worse, which led to the decision to abandon geometry factors for this band. In the strong CO_2 band (lower panel), the original calibration shows a difference of more than 12 ppm between the two intensity states. The revised calibration shows enormous improvement, with a difference of about 0.8 ppm.

V. OCO Noise Model

A key parameter in most retrievals involving OCO data, for instance, the retrieval of carbon dioxide using an optimal estimation approach (e.g., [8], [12]), is the instrument noise level. For an imaging spectrometer like OCO, the radiometric noise N in a given instrument channel can be assumed to behave solely on the measured intensity I according to

$$N(I) = I_{\max} \cdot \sqrt{\frac{I}{I_{\max}} \cdot C^2_{\mathrm{photon}} + C^2_{\mathrm{background}}} \qquad (11)$$

where $I_{\max}$ is the maximum measurable signal, defined by instrument specification. For the O_2 A-band and the weak and strong CO_2 bands, these values are 370, 65, and 15 $\mathrm{W} \cdot \mathrm{m}^{-2} \cdot \mu\mathrm{m}^{-1} \cdot \mathrm{sr}^{-1}$, respectively. They roughly represent values 5%–10% higher than the intensities due to nadir observation of an optical depth 60 cloud illuminated by the sun at a zenith angle of 20°. $C_{\mathrm{background}}$ is a constant that represents the contribution of dark noise, and C_{photon} is a constant that describes the coupling of the illumination level to the noise. This second parameter captures the effective instrument performance (including such terms as transmission, focal ratio, obscurations, and quantum efficiency of the detectors).

For each spectral sample, the noise was measured for each illumination level of the integrating sphere (Fig. 9). The C_{photon} and $C_{\mathrm{background}}$ parameters were then derived by a least squares fit for each channel, footprint, and band of the instrument; an example of this is shown in Fig. 9(a). The SNR has two regimes: linear for very low radiance and square root for high radiance. The OCO instrument was sensitive enough that most of the dynamic range was in the square root (photon-limited) regime. After the fits for C_{photon} and $C_{\mathrm{background}}$ for all instrument channels, the noise could then be calculated for arbitrary intensity I using (11). Fig. 9(b) shows a graph of the SNR versus I (expressed as a percentage of $I_{\max}$) for each OCO band.

These are the SNRs for each actual instrument channel. However, because OCO was spectrally oversampled by a factor of approximately 2.5, the noise per independent spectral sample is a factor of ∼1.6 lower. Even in the case of a relatively dim scene, such as albedo 0.05 with a solar zenith angle of 60°, the SNR values per independent spectral sample are 310, 340, and 230 for the three OCO bands. This met the mission requirements for the weak and strong CO_2 bands, but slightly missed the requirement in the O_2 A-band.

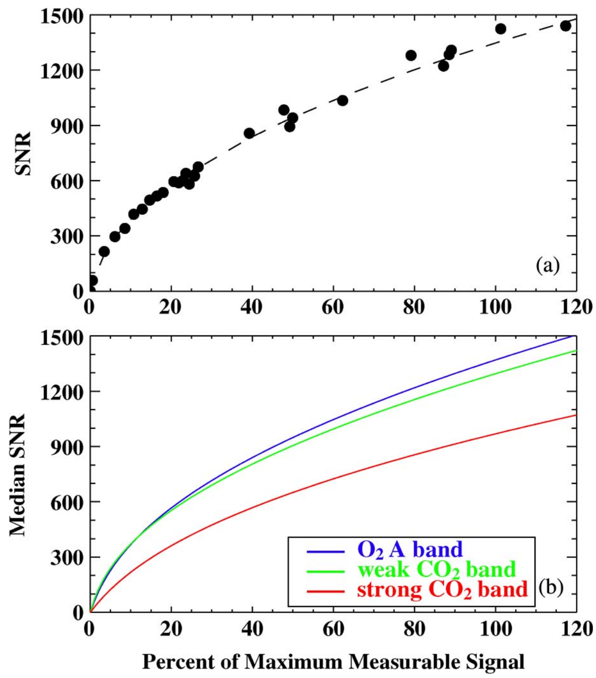

Fig. 9. SNR for the OCO flight instrument. (a) (Filled circles) SNR for a single channel near the center of the weak CO_2 band at a variety of intensity levels taken during preflight calibration and (dashed line) the resulting SNR model based on a fit to the noise model of (11). (b) Median SNR across all channels in each of the three OCO bands. The O_2 A-band is shown in blue, the weak CO_2 band in green, and the strong CO_2 band in red.

VI. Conclusion

This paper has described the radiometric calibration of the original OCO instrument in terms of both its dark current response and gain coefficients. An initial calibration suffered from incorrect assumptions about the calibration test setup, specifically relating to the photodiodes used for the calibration, as well as uniformity of the intensity field within the integrating sphere. Improvements to the photodiode response and integrating sphere models led to large improvements in the accuracy of the calibration, assessed through the matador test in terms of both the constancy of the intensity ratio as well as of the corresponding retrievals of geophysical variables.

Undoubtedly, there is still room for improvement in all three bands in terms of characterizing instrumental nonlinearities. This is evident in both the residual slope of Fig. 7 and the differences in retrievals for the different intensity levels evident in Fig. 8. These states differed by a factor of about 2 in continuum intensity. For actual space-based observations, OCO was expected to make X_{CO_2} retrievals for intensity levels that ranged over a factor of more than 20. Therefore, potentially larger errors due directly to detector nonlinearity could be expected, leading to regional biases on the order of 1 ppm or greater.

The problems with the integrating sphere data were due to the limited time frame available for testing and will be corrected for the preflight calibration of the upcoming OCO-2 mission, scheduled to launch in early 2013. In particular, the photodiodes will be extremely well temperature controlled, and their response will be accurately characterized over the necessary range of intensity levels. Furthermore, the integrating sphere will be made more reflective in the strong CO_2 band. This should lead to a sufficiently accurate calibration and contribute to the success of the OCO-2 mission.

Acknowledgment

The authors would like to thank L. Wayne of JPL for the information on the calibration setup and help in diagnosing the strong CO_2 band photodiode issues, B. Hancock of JPL for the discussions on the W-pattern, J. McDuffie for the computing help, and all the JPL employees who worked tirelessly to acquire the OCO TVAC data. A portion of the research described in this paper was carried out at the JPL, California Institute of Technology, under a contract with the National Aeronautics and Space Administration (NASA). The Colorado State University contributions to this work were carried out under NASA Contract 1280999.

References

[1] D. Crisp, R. M. Atlas, F.-M. Breon, L. R. Brown, J. P. Burrows, P. Ciais, B. J. Connor, S. C. Doney, I. Y. Fung, D. J. Jacob, C. E. Miller, D. O'Brien, S. Pawson, J. T. Randerson, P. Rayner, R. J. Salawitch, S. P. Sander, B. Sen, G. L. Stephens, P. P. Tans, G. C. Toon, P. O. Wennberg, S. C. Wofsy, Y. L. Yung, Z. Kuang, B. Chudasama, G. Sprague, B. Weiss, R. Pollock, D. Kenyon, and S. Schroll, "The Orbiting Carbon Observatory (OCO) mission," *Adv. Space Res.*, vol. 34, no. 4, pp. 700–709, 2004.

[2] D. Crisp and C. Johnson, "The Orbiting Carbon Observatory mission," *Acta Astronaut.*, vol. 56, no. 1/2, pp. 193–197, Jan. 2005.

[3] J. O. Day, C. W. O'Dell, C. Bruegge, and R. Pollock, "Preflight spectral calibration of the Orbiting Carbon Observatory," *IEEE Trans. Geosci. Remote Sens.*, to be published.

[4] F. Sakuma, C. Bruegge, D. Rider, D. Brown, S. Geier, S. Kawakami, and A. Kuze, "OCO/GOSAT preflight cross-calibration experiment," *IEEE Trans. Geosci. Remote Sens.*, vol. 48, no. 1, pp. 585–599, Jan. 2010.

[5] R. Haring, R. Pollock, B. Sutin, and D. Crisp, "Current development status of the Orbiting Carbon Observatory instrument optical design," *Proc. SPIE*, vol. 5883, no. 1, p. 588 30C, 2005.

[6] D. M. O'Brien, R. Pollock, I. Polonsky, and M. Rogers, "Identification and correction of residual image in the O_2 A-band of the Orbiting Carbon Observatory," *IEEE Trans. Geosci. Remote Sens.*, to be published.

[7] C. D. Rodgers, *Inverse Methods for Atmospheric Sounding: Theory and Practice*. Singapore: World Scientific, 2000.

[8] H. Bösch, G. C. Toon, B. Sen, R. A. Washenfelder, P. O. Wennberg, M. Buchwitz, R. de Beek, J. P. Burrows, D. Crisp, M. Christi, B. J. Connor, V. Natraj, and Y. L. Yung, "Space-based near-infrared CO_2 measurements: Testing the Orbiting Carbon Observatory retrieval algorithm and validation concept using SCIAMACHY observations over Park Falls, Wisconsin," *J. Geophys. Res.*, vol. 111, no. D10, p. D23 302, Dec. 2006.

[9] L. S. Rothman, I. E. Gordon, A. Barbe, D. C. Benner, P. F. Bernath, M. Birk, V. Boudon, L. R. Brown, A. Campargue, J. Champion, K. Chance, L. H. Coudert, V. Dana, V. M. Devi, S. Fally, J. Flaud, R. R. Gamache, A. Goldman, D. Jacquemart, I. Kleiner, N. Lacome, W. J. Lafferty, J. Mandin, S. T. Massie, S. N. Mikhailenko, C. E. Miller, N. Moazzen-Ahmadi, O. V. Naumenko, A. V. Nikitin, J. Orphal, V. I. Perevalov, A. Perrin, A. Predoi-Cross, C. P. Rinsland, M. Rotger, M. Šimečková, M. A. H. Smith, K. Sung, S. A. Tashkun, J. Tennyson, R. A. Toth, A. C. Vandaele, and J. Vander Auwera, "The HITRAN 2008 molecular spectroscopic database," *J. Quant. Spectrosc. Radiat. Transf.*, vol. 110, no. 9/10, pp. 533–572, Jun./Jul. 2009.

[10] H. Tran and J. Hartmann, "An improved O_2 A band absorption model and its consequences for retrievals of photon paths and surface pressures," *J. Geophys. Res.*, vol. 113, p. D18 104, Sep. 2008.

[11] J. Hartmann, H. Tran, and G. C. Toon, "Influence of line mixing on the retrievals of atmospheric CO_2 from spectra in the 1.6 and 2.1 μm regions," *Atmos. Chem. Phys. Discuss.*, vol. 9, no. 1, pp. 4873–4898, Feb. 2009.

[12] T. Yokota, Y. Yoshida, N. Eguchi, Y. Ota, T. Tanaka, H. Watanabe, and S. Maksyutov, "Global concentrations of CO_2 and CH_4 retrieved from GOSAT: First preliminary results," *SOLA*, vol. 5, pp. 160–163, 2009.

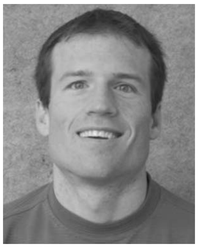

Christopher W. O'Dell received the Ph.D. degree in physics from the University of Wisconsin, Madison, in 2001, where he studied the cosmic microwave background radiation.

After his postdoctoral positions in both astronomy and microwave remote sensing, he joined the research staff at the Colorado State University, Fort Collins, in 2007, where he is currently a member of the Cooperative Institute on Research in the Atmosphere. His research concerns the remote sensing of climatically important atmospheric variables such as water vapor and carbon dioxide.

Jason O. Day received the Ph.D. degree in atomic physics from the University of Wisconsin, Madison.

From 2008 to 2009, he was a Postdoctoral Fellow with the Orbiting Carbon Observatory Team, National Aeronautics and Space Administration. He is currently an AAAS Science and Technology Policy Fellow with the Division of Atmospheric and Geospace Sciences, National Science Foundation, Arlington, VA.

Randy Pollock received the B.S. degree in engineering and applied science from the California Institute of Technology, Pasadena, in 1991.

He is currently an Instrument Architect with the Orbiting Carbon Observatory, Jet Propulsion Laboratory, National Aeronautics and Space Administration, Pasadena.

Carol J. (Kastner) Bruegge received the Ph.D. degree in optical sciences from the University of Arizona, Tucson, in 1985.

She is currently with the Jet Propulsion Laboratory, California Institute of Technology, Pasadena, CA, where she was a member of the Earth Observing System Multiangle Imaging Spectroradiometer Team from 1988 to 2003, is a member of the Orbiting Carbon Observatory Science Team, and has been the Principal Investigator of the LED Spectrometer Automatic Vicarious Calibration Facility and also the First International Satellite Land Surface Climatology Program Field Experiment, which is a ground-truth hydrology experiment conducted from 1987 through 1992.

Denis M. O'Brien received the M.Sc. degree in theoretical physics from the Australian National University, Acton, Australia, and the Ph.D. degree in mathematical physics from the University of Adelaide, Adelaide, Australia.

After his postdoctoral positions in Scotland and Australia, he was with the Commonwealth Scientific and Industrial Research Organization of Australia, where his focus was radiation, remote sensing, and instrumentation. In 2004, he moved to Colorado State University, Fort Collins, as a Senior Research Scientist. He is a member of the Orbiting Carbon Observatory and Atmospheric Carbon Observations from Space Science Teams.

Rebecca Castano received the Ph.D degree in electrical engineering from the University of Illinois with her dissertation in the area of computer vision.

She currently is the Science Algorithms Manager for the Atmospheric Carbon Dioxide from Space (ACOS) task and the OCO-2 mission. In addition she is currently an Assistant Manager for Technology Development and Infusion for the Instrument Software and Science Data Systems Section at the Jet Propulsion Laboratory, Pasadena, CA. She has been advancing the state of the art in autonomous planetary science for over a decade and has authored numerous publications in the field.

Irina Tkatcheva received the M.S. degree in physics from Moscow State University, Moscow, Russia, in 1991 and the B.S. degree in computer science from California State University, Los Angeles, in 1995.

She is currently a Software Engineer with the Jet Propulsion Laboratory, California Institute of Technology, Pasadena, CA.

Charles E. Miller received the B.S. degree in chemistry from Duke University, Durham, NC, and the Ph.D. degree in physical chemistry from the University of California, Berkeley.

He is currently with the Earth Atmospheric Science Division, Jet Propulsion Laboratory, California Institute of Technology, Pasadena, CA, where he is currently the Deputy Project Scientist for the second Orbiting Carbon Observatory (OCO-2) mission.

David Crisp received the Ph.D. degree from Princeton University, Princeton, NJ in 1984.

He is currently an Atmospheric Physicist and a Senior Research Scientist with the Jet Propulsion Laboratory, California Institute of Technology, Pasadena, CA. He was the Principal Investigator of the Earth System Science Pathfinder Orbiting Carbon Observatory mission, which is the National Aeronautics and Space Administration's first dedicated carbon dioxide measurement mission. He is currently serving as the Science Lead for the recently approved OCO-2 mission.